Study of creep damage in a 10.86% Cr heat resistant steel using synchrotron X-ray microtomography

Gupta, C.
Mechanical Metallurgy Division, Materials Group, Bhabha Atomic Research Centre | Department of Mechanical Engineering, Toyohashi University of Technology

Toda, Hiroyuki
2Department of Mechanical Engineering, Toyohashi University of Technology

Schlacher, C.
Institute for Materials Science and Welding, Graz University of Technology

Mayr, P.
Institute of Joining and Assembly, Chemnitz University of Technology

他

出版情報：794, pp.476-483, 2013-09-01. Trans Tech Publications
バージョン：
権利関係：

Study of Creep damage in a 10.86% Cr Heat Resistant Steel using Synchrotron X-ray Microtomography

C. Gupta[1,2,a], H. Toda[2], C. Schlacher[3], P. Mayr[4], C. Sommitsch[3], K. Uesugi[5], Y. Suzuki[5], A. Takeuchi[5], M. Kobayashi[2]

[1]Mechanical Metallurgy Division, Materials Group, Bhabha Atomic Research Centre, Mumbai - 400085, India.
[2]Department of Mechanical Engineering, Toyohashi University of Technology, Toyohashi 441-8150, Japan.
[3]Institute for Materials Science and Welding, Graz University of Technology, Kopernikusgasse, 24/I A-8010 Graz, Austria.
[4]Institute of Joining and Assembly, Chemnitz University of Technology, reichenhainerStrasse 70, 09126 Chemnitz, Germany.
[5]Japan Synchrotron Radiation Research Institute, Sayo-gun, Hyogo 679-5198, Japan.

[a]cgupta@barc.gov.in(corresponding author)

Keywords: Heat Resistant Steel, Creep Cavitation, Synchrotron Microtomography

Abstract. Synchrotron X-ray micro-tomography (SR-µCT) scans have been carried out on sample coupons extracted from fracture specimens of a 10.86% Cr heat resistant steel exposed to creep deformation at 873K over stresses of 120, 150 and 180 MPa. The 3D cavitation characteristics in terms of void volume fraction, number density and size distribution as a function of the applied stress has been determined by quantitative analysis of reconstructed tomography slice datasets. The relationship between heterogeneous spatial distributions of creep voids and variation in rupture life has been explored in terms of microstructural specific nucleation sites during the onset of creep embrittlement.

Introduction

Creep fracture in materials is mainly due to cavity nucleation and growth [1]. In heat resistant steels creep plasticity and fracture are intimately connected to the evolution of microstructure during high temperature exposure. Advanced heat resistant steels that are used for the ultra-super critical power plant components derive their creep resistance from the fine scale microstructure (martensitic laths with sub-grain structure) and from the presence of precipitates located at various internal interfaces (prior austenite, packet & lath and sub-grain boundaries) [2]. During high temperature exposure, coarsening of the substructure network occurs towards the stress dependent equilibrium sub-grain values. Concomitantly, the evolution of metastable precipitates in terms of size and composition along with the appearance of intermetallic precipitates such as Laves phase and complex nitride Z phase take place [3]. These changes govern the onset of cavitation behaviour and the progress of creep damage in advanced tempered martensitic steels. In these steels, the creep test results evaluated in strain rate – strain format, reveals that the creep rate first reaches minimum within a short strain interval. With continued exposure to stress, the creep rate increases due to the microstructure coarsening processes mentioned above and finally large-scale cavitation occurs, which leads to fracture. The research into the cavitation behaviour in heat resistant steels and establishing its relationship to the underlying state of the crept microstructure is vital in order to have a fundamental understanding of the mechanisms of creep fracture. These would ultimately lead to strategies to prolong the creep life of tempered martensitic steels for ultra-supercritical power plants.

The techniques widely used to study cavitation have been mainly destructive techniques (SEM and TEM, SEM-OIM, TEM along with EDX and nano-hardness measurements), which are in 2D [4]. The

characterisation of creep damage using these techniques is limited by firstly, the artefacts arising from the destructive sample preparation techniques. Secondly, these techniques are unable to image the complex shape, connectivity and spatial distribution of voids [5]. The X-ray micro-tomography technique using large synchrotron sources (eg. SPring-8, ESRF, APS) offers distinct advantages (non-destructive nature, and probing in bulk) due to which recent literature is replete with examples to investigate the fracture and fatigue behaviour of engineering materials [5]. Recently it has been possible to use the technique for characterising damage in dense absorbent material to X-rays such as steels at micro-meter resolution length scale [6]. An example of this is a recent investigation on the development of creep damage (voids and cracks) in a Fe-Ni-Cr fully austenitic steel using synchrotron beam line Spring-8, which provided quantitative characterization of the void content in the as-cast and ex-service variants of the material [7]. In this paper, the high resolution (~1 μm) synchrotron micro-tomography (SR-μCT) available at beamline BL20XU, SPring-8, has been used to characterise evolution of voids due to creep deformation in advanced 9-12%Cr tempered martensitic steel. The aim of the investigations was to characterise the spatial distribution of the creep voids with increasing creep exposure times.

Experimental

The commercial steel selected for the investigation is a 10.86% Cr steel containing 610 ppm Nb, 100 ppm B, 240ppm N and 260 ppm Al. The steel has been exposed to creep deformation after quenching and tempering treatment involving austenitising at 1373 K for 8 hours, followed by tempering at 1003 K for 36 hours. The stress rupture tests were carried out with periodic interruptions to measure creep strain, until failure at 873 K during loading at nominal initial stress range of 120 – 180 MPa. The diameter on companion specimens was varied in the range 7.64-9.65 mm, to define the prescribed level of stress to be imposed under a constant on-axis load of 8.25 kN. The nominal diameter to gauge length ratio was kept at five. In order to investigate the attendant damage using SR-μCT, sample coupons with a square cross-section of about 300x300 μm^2 were extracted from selected crept specimens near (less than 5 mm) to the fracture surface. Such small sample coupons were used for the ex-situ tomography examination as the absorption of steels to X-rays are very high. The SR-μCT on the extracted samples was performed at the undulator beamline BL20XU of the SPring-8. A monochromatic X-ray beam produced by a liquid nitrogen-cooled Si (511) - (333) double crystal monochromator, was tuned to produce a beam of energy 40 keV. An image detector system, placed 110 mm from the sample, consisted of a cooled 4000 (H) × 2624 (V) element CCD camera (effective pixel size of the camera: 5.9 μm, used in 2 x 2 binning mode), a LSO:Ce scintillator (Lu_2SiO_5:Ce) and a relay lens (×20). In total, 1500 radiographs, scanning 180 degrees, were obtained in 0.12-degree increments. Theoretical limit of this projection-type SR-μCT set-up is approximately 1 μm, which is determined primarily by inevitable image blurring caused by the Fresnel diffraction, the diffraction limit of visible light and the spatial resolution of a scintillator [6]. Isotropic voxels (a volume element in 3D space) with 0.5 μm edges were achieved in the reconstructed slices that were at least necessary to achieve the 1 μm spatial resolution [6]. A convolution back projection algorithm was used for achieving the reconstruction and the analysis of the reconstructed slices for various damage characteristics were executed in customized software.

In order to extract the creep cavities for analysis, a local threshold of grey value was assigned and only those greater than 3^3 connected voxels were selected so that cavities smaller than 1.5 μm diameter were ignored which made the determination of the 3D cavitation parameters conservative. It is to be mentioned here that this minimum threshold voxel limit of void size used for quantitative analysis is more than twice that used by Sket et. al. [8] for ex-situ investigations on creep deformed E911 steel (which was 8 voxel). The analysis software implemented the marching cubes algorithm to determine the number, volume, surface area and co-ordinates of the centre of mass of each void present in the reconstructed region of interest.

Results and Discussion

The creep test results are summarized in figure 1(a) in the form of variation of minimum creep rate ($\dot{\varepsilon}_{min}$), Larson-Miller (LM) parameter and rupture ductility with initial stress. A linear relationship is clearly evident between $\dot{\varepsilon}_{min}$ and LM parameter, and the applied stress. The stress exponent has been calculated from the $\dot{\varepsilon}_{min}$ - σ plot as 17.8. This value is in the range typical for precipitation hardened materials in the high stress regime where the tertiary creep governs creep life [1]. The linear relationship with single slope within the applied stress range for both $\dot{\varepsilon}_{min}$ and LM parameter suggests that the cavitation led increase in creep rate is predominately restricted in the tertiary regime [1]. Previous studies opine that formation of creep voids commence from early stages in the creep life of CrMoV steels, by nucleation of nano-meter sized cavities [1]. However, considering the fact that $\dot{\varepsilon}_{min}$ - σ plot is linear, the effect of the presence such cavities seems to be minimal in the stages prior to tertiary creep regime of the steel.

Figure 1. (a) Variation of minimum creep rate, Larson-Miller parameter, and rupture ductility at the selected creep stresses where microtomography has been carried out. (b) Variation of fraction of creep life spent in cavitation dominated with initial applied stress during creep test. The points shown in black are the creep condition where microtomography has been carried out ex-situ.

In tempered martensitic steels the tertiary regime can be distinguished into two regions – a coarsening dominated region and a cavitation-dominated region. As enhanced creep rates would mean rapid elongation over short time, it is reasonable to propose that a simple tangent intersection in the elongation-time plot obtained from creep test (as shown in the inset of figure 1(b)) can estimate the point where the cavitation dominated region commences. The plot of the ratio of the cavitation dominated region in tertiary stage to the creep life as a function of applied stress is shown in figure 1(b) as plot of variation t_D/t_F ratio with applied stress. The numerator (t_D) of the ratio represents the time taken from the tangent intersection point to fracture and the denominator (t_F) represents the total creep life. It is clearly seen that there is a sharp decline in the ratio as creep stress reduces from 180 to 120 MPa. This conclusively shows in this steel that as the creep exposure time increases at lower stress there is decrease in the fraction of the creep life devoted for cavitation damage before fracture. It is of significance to point out that the fracture surface observations after creep in the stress ranges 120-180 MPa at 873 K of the steel was found to be increasingly inter-granular below 165 MPa. The presence of inter-granular fracture is an indication of creep brittleness and could be responsible for the decrease in the t_D/t_F ratio with stress.

(a) (b)

Figure 2 (a) 3D rendering of the region of interest of the sample subjected to creep at 120 MPa. (b) Close up view of the typical morphology of the creep voids found in the dataset in (a)

The 3D rendering of the reconstructed slices obtained from SR μCT scans on the sample tested at stress 120 MPa is shown in figure 2(a). It can be clearly seen that the creep damage is

heterogeneously distributed in the reconstructed volume of interest. Appearance of regions containing void clusters can be clearly distinguished. The presence of large complex shaped voids as well as multi-lobed voids can be clearly seen. Figure 2(b) shows a few close up renderings of these complex voids visualized in the sample exposed to creep for the longest time. These range from being multi-lobed chain of voids to a complex void cluster near a large oblate shaped void. The observation of multi-lobed morphology of voids suggests the operation of void coalescence processes in their formation.

The results from the quantitative analyses of the reconstructed images applied to determine the characteristics of cavitation are shown in figure 3. It is seen that on reducing the stress from 180 to 150 MPa, the number density of voids increases without significant variation in its volume fraction and average void size. This trend suggests that an increase in cavitation results from an increase in the nucleation of new creep voids at these stresses. This is inferred from the fact that if void growth and coalescence dominates over nucleation, then it is expected that the void volume fraction should increase at the expense of number density. At the lowest stress, (i.e. 120 MPa) however, there has been nearly three-fold increase in volume fraction along with slight increase in the average diameter of voids and a significant upswing in the number density curve. This implies the growing influence of void growth and coalescence mechanisms. This is also corroborated by the presence of many of complex shaped large voids at the lowest stress (figure 2 (b)). The observation that at the lowest stress the void morphology consisted of both ellipsoid shapes as well as complex multi-lobed shapes strengthens the argument of the presence of strong coalescence mechanisms as creep brittleness is approached.

The analysis of the void size distribution is shown in figure 3(d). It is clearly seen that as the creep exposure times increase (or the creep stress reduces) the peak frequency of void size both increases in magnitude and also shifts towards larger void size values. This result lends support to the suggestion that at long creep exposures intense cavitation comprises of nucleation of new voids along with increasing influence of void coalescence. This interpretation stems from the observation that the size distribution shows first an increase in peak frequency and then at the lowest stress shifts to the right.

Figure 3. Stress dependent variation of (a) number density (b) void diameter (c) void volume fraction (d) void size distribution.

The functional relationship between the intrinsic cavitation characteristics and macroscopic creep ductility over the stress range 120 – 180 MPa can now be quantified. The plot between void volume fraction and number density with rupture ductility is shown in figure 4. It can be clearly seen that these cavitation characteristics undergo a transition as the creep ductility is reduced in the stress range 120 – 150 MPa. At rupture ductility ranges above 14%, which was obtained at the stresses 150 and 180 MPa, both void volume fraction and number density are found to be at low levels. At stress of 120 MPa where a significant drop in the rupture ductility has been found, these cavitation parameters dramatically increase in an exponential manner. The exponential fit correlating the dependence of rupture ductility on the cavitation parameters (void volume fraction, ν and number density, η) is given below:

$$\nu = 165.76 + 6.7x10^{8} \exp(-1.91\Lambda) \quad (1)$$

$$\eta = 0.399 + 7.0 \exp(-0.33\Lambda) \quad (2)$$

where ν is the void volume fraction in ppm, η is the number density in $10^{-5}\mu m^{-3}$ and Λ is the rupture ductility in %. These parameters provide a quality of fit (R^2) value of 0.94.

Figure 4. (a) Variation of cavitation characteristics with rupture ductility (b) Distribution of total void volume over the void size.

Figure 4(b) shows the plot of total void volume as a function void size for each of the datasets quantitatively analysed of samples crept to failure at stress range 120 – 180 MPa. It is seen that the total void volume for each dataset as a function of size range first increases until it reaches near to its respective peak frequency size range. Subsequently, at larger void sizes the total void volume first sharply drops, and then either continues to display a gradual downward trend or an upward trend depending on the stress level during the creep testing. In all cases intermittent peaks are prominently seen in the void size ranges beyond the respective peak frequency size. These peaks suggest that both growth of individual voids and coalescence existing voids occurs for the associated void size ranges. These trends suggest that at the void size range below the peak frequency size range there could be predominately rapid growth of the voids as both total void volume and average void volume increase. The larger void sizes than the peak frequency size could be formed mostly by a combination of growth and coalescence of voids. It is to be noted that this view restricts the computation of void growth rate for void size range up to only about 4 μm (depending the respective creep stress). This is consistent with the studies of Wu and Sandström [9] where the growth rate of creep voids up to 2.5 μm in Cr-Mo-V steel at 600°C were reported. The trends observed in the quantitative characteristics of cavitation with stress, exposure time and void size as well as the morphology of the creep voids at 120 MPa, suggests that the increase in cavitation at the lowest stress occurs due to both nucleation of new voids as well as growth and coalescence of the voids formed perhaps at the early stages of the creep life of the steel.

(a) (b)

Figure 5. Expanded 3D rendering of the region of intense cavitation in datasets crept at (a) 150MPa and (b) 120 MPa.

The rendered 3-D volume expanded near to regions of high density of cavitation for the samples exposed to creep stress of 150 and 120 MPa are shown in figure 5. The contrast in the spatial alignment of the chains of voids of the two cases is clearly evident, which have been emphasized by the black lines in the images. These lines represent the voids aligned inside the reconstructed region seen visually after 3D rendering. The dataset obtained from the sample crept at 150 MPa shows very restrictive alignments. In the case of 120 MPa the cavitation is far more proliferated. From the fact that the austenite grain size is about 600 μm in the crept microstructure, the aligned voids for the sample crept at 120 MPa, could be interpreted as being interfaces within the grain interior such as packet or lath boundaries. This is because the spacing between the rows of aligned voids clearly is much less than the prior austenite grain size. This suggests that as cavitation proliferates at lower stresses, the grain interior interfaces show significant cavitation. This observed trend of the grain

interior interfaces to cavitate at lower stress, where the creep brittleness increases, has been also reported for other CrMoV steels [10].

The present work through the application of micro-tomography provides a basis for understanding of the pattern of cavitation as creep brittleness is approached in the steel at 873K. While earlier studies on CrMoV steels reported the presence of creep voids at both the grain boundary and its interior, an unambiguous quantification using non-invasive 3D techniques of the extent of cavitation and its relation to the rupture ductility within the stress range 120-180 MPa for this steel was lacking. The study revealed a complex non-linear functional relationship between these two parameters for this CrMoV steel, which could be considered as the fundamental nature of the cavitation behaviour in this class of steels. Further, the increase in cavitation at smaller applied stress in this steel is observed to be due to nucleation at the grain interior interfaces. Thus, a transition of cavitation with applied stress during creep in this steel occurs from being predominately restricted at the grain boundary at stresses 150 MPa and above, to progressively proliferate the grain interior interfaces at lower stresses. This change in cavitation behaviour in the heat resistant steel most likely results in the increase in creep brittleness as the applied stress is reduced. This understanding has important implications for developing strategies to improve the creep resistance by reducing/delaying the cavity nucleation at grain interior interfaces. Further, the study indicates that there is a need to account for the role of cavitation at the grain interior interfaces in hastening creep rupture in this class of steels.

Summary

The creep damage studies in a 10.86% Cr heat resistant steel using high resolution synchrotron micortomography technique reveal a direct relationship between increase of cavitaion and redution in creep ductility when exposed to low stresses at 873K where there is transition from transgranular to intergranular failure. It appears from the pattern of creep damage developed in the 3D datasets of samples tested at 180 MPa, 150 MPa and 120 MPa, that cavitation at grain interior interfaces could play a pivotal role in hastening this transition of failure mode.

References

[1] M. E. Kassner, Fundamentals of Creep in Metals and Alloys, Second ed., Elsevier, UK, 2009.
[2] F. Abe, Precipitate design for creep strengthening of 9% Cr tempered martensitic steel for ultra supercritical power plants, Sci. Technol. Adv. Mater. 9 (2008) 1-15.
[3] A. Aghajani, C. H. Sommen, G. Eggler,On the effect of long term creep on the microstructure of a 12% Chromium tempered martensitic ferritic steel, Acta. Mater, 57 (2009) 5093-5106.
[4] K. Fujiyama, K. Mori, T. Matsunaga, H. Kimachi, T. Saito, T. Hino, R. Ishhii,Creep damage assessment of high chromium heat resistant steels and weldments, Mater. Sci. Eng. A501-511 (2009) 195-201.
[5] S. R. Stock, MicroComputed Tomography – Metholodology and Applications, CRC Press USA 2009.
[6] H. Toda, F. Tomizato, M. Ziessmann, Y. Besel, K. Uesugi, A. Takeuchi, Y. Suzuki, M. Kobayashi, B.-F. Foit, High resolution observation of steel using X-ray tomography technique, ISIJ 52 (2012) 517-523.
[7] K. S. Cheong, K. J. Stevens, Y. Suzuki, K. Uesugi, A. Takeuchi, The effects of microstructure on creep behavior – A study through synchrotron X-ray microtomography, Mat. Sci. Eng. A513-514 (2009) 222-227.
[8] F. Sket, K. Dzieciol, A. Borbely, A. R. Pyzalla, K. Maile, R. Scheck, Microtomographic investigation of damage in E911 steel after long term creep, Mater. Sci. Eng. A528 (2010) 103-111.

[9] R. Wu, R. Sanström, Creep cavity nucleation and growth in 12Cr-Mo-V steel, Mater. Sci. Tech. 11 (1995) 579-588.
[10] G. Eggeler, J. C. Earthman, N. Nilsvang, B. Ilshner, Microstructure study of creep rupture in a 12% chromium ferritic steel, Acta. Metall. 37 (1989) 49-59.

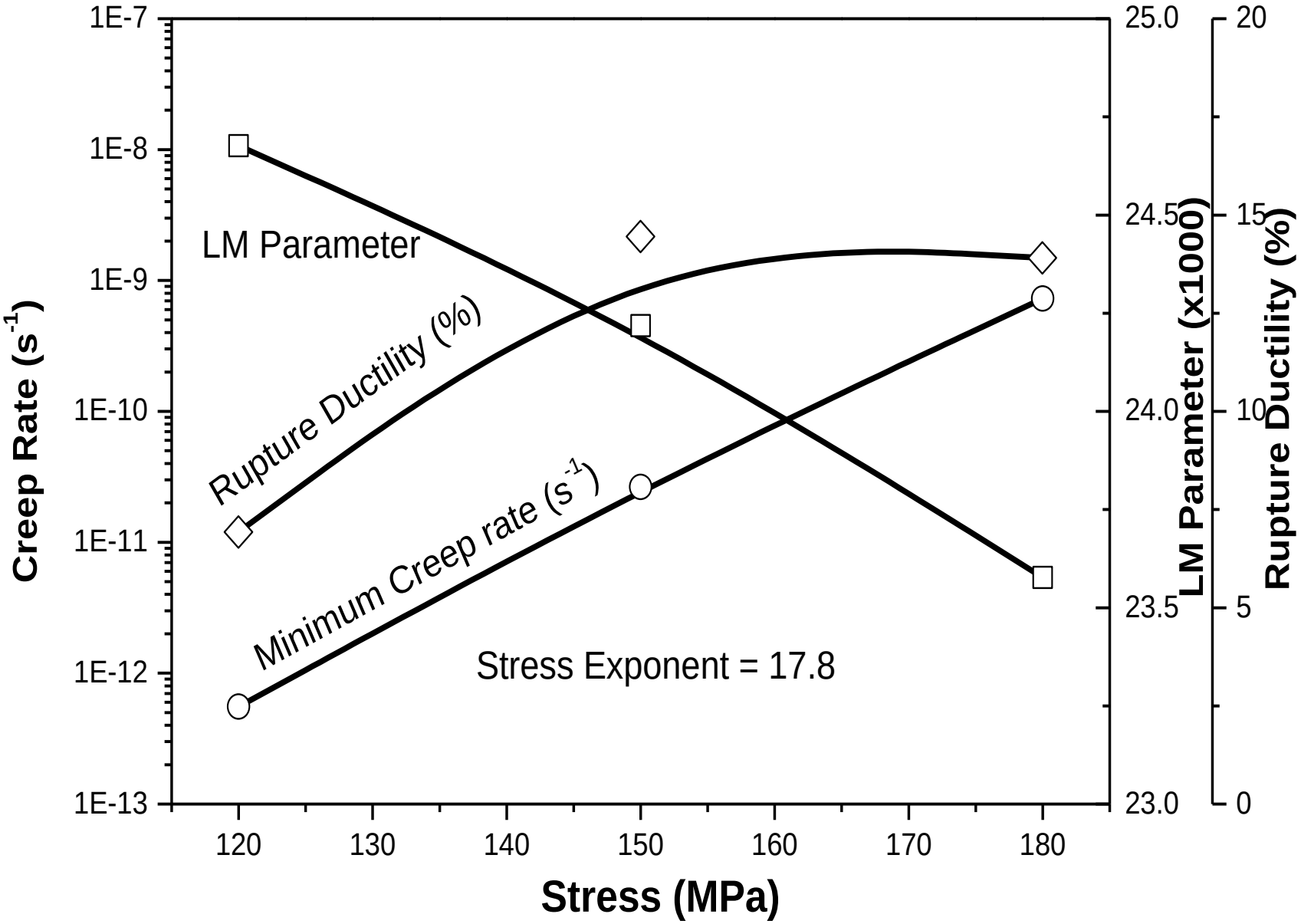
1E-7
1E-8
1E-9
1E-10
1E-11
1E-12
1E-13
Creep Rate (s-1)
25.0
24.5
24.0
23.5
23.0
LM Parameter (x1000)
20
15
10
5
0
Rupture Ductility (%)
120
130
140
150
160
170
180
Stress (MPa)
LM Parameter
Rupture Ductility (%)
Minimum Creep rate (s-1)
Stress Exponent = 17.8

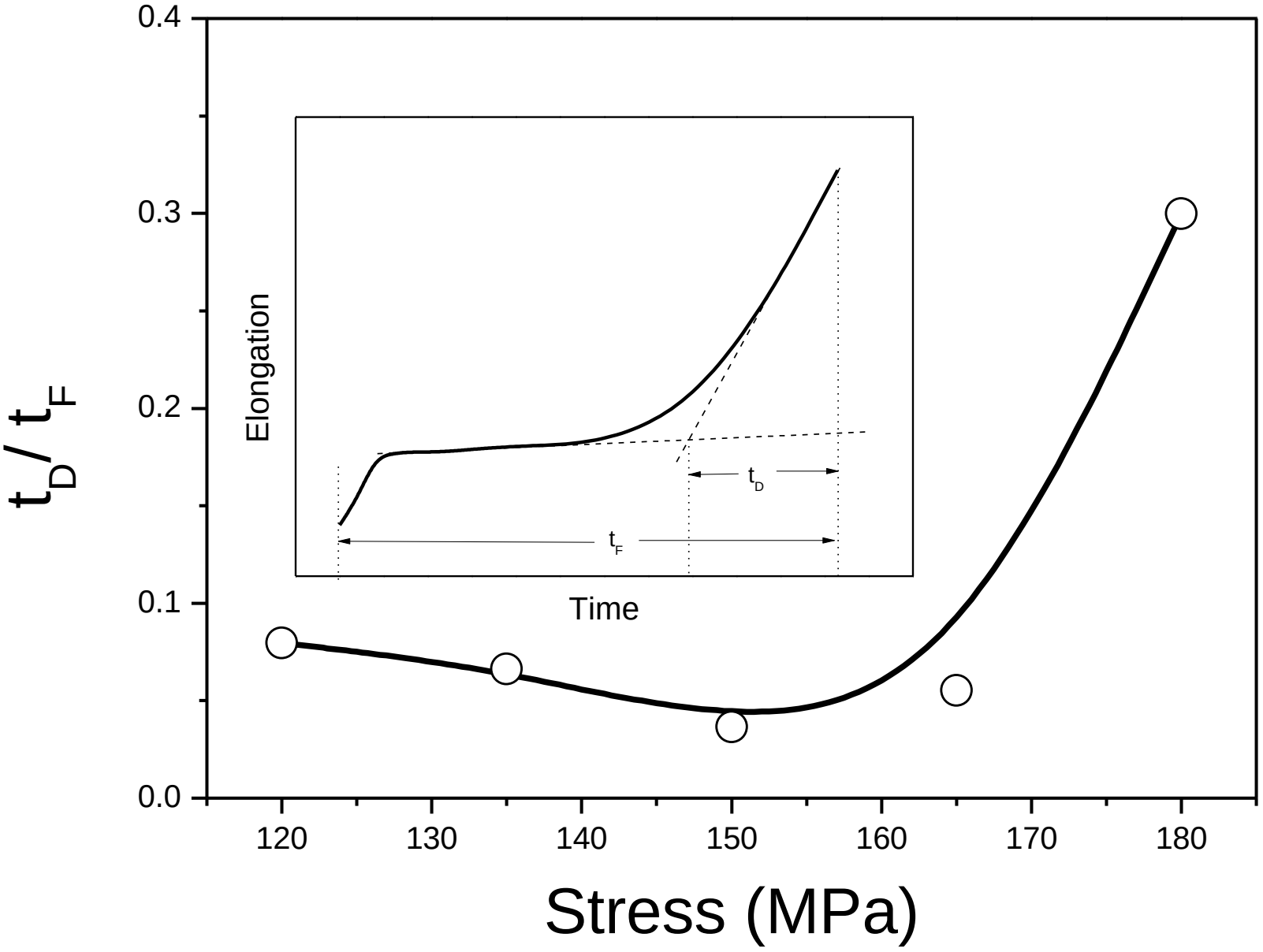
0.4
0.3
0.2
0.1
0.0
t_D / t_F
120
130
140
150
160
170
180
Stress (MPa)
Elongation
Time
t_D
t_F

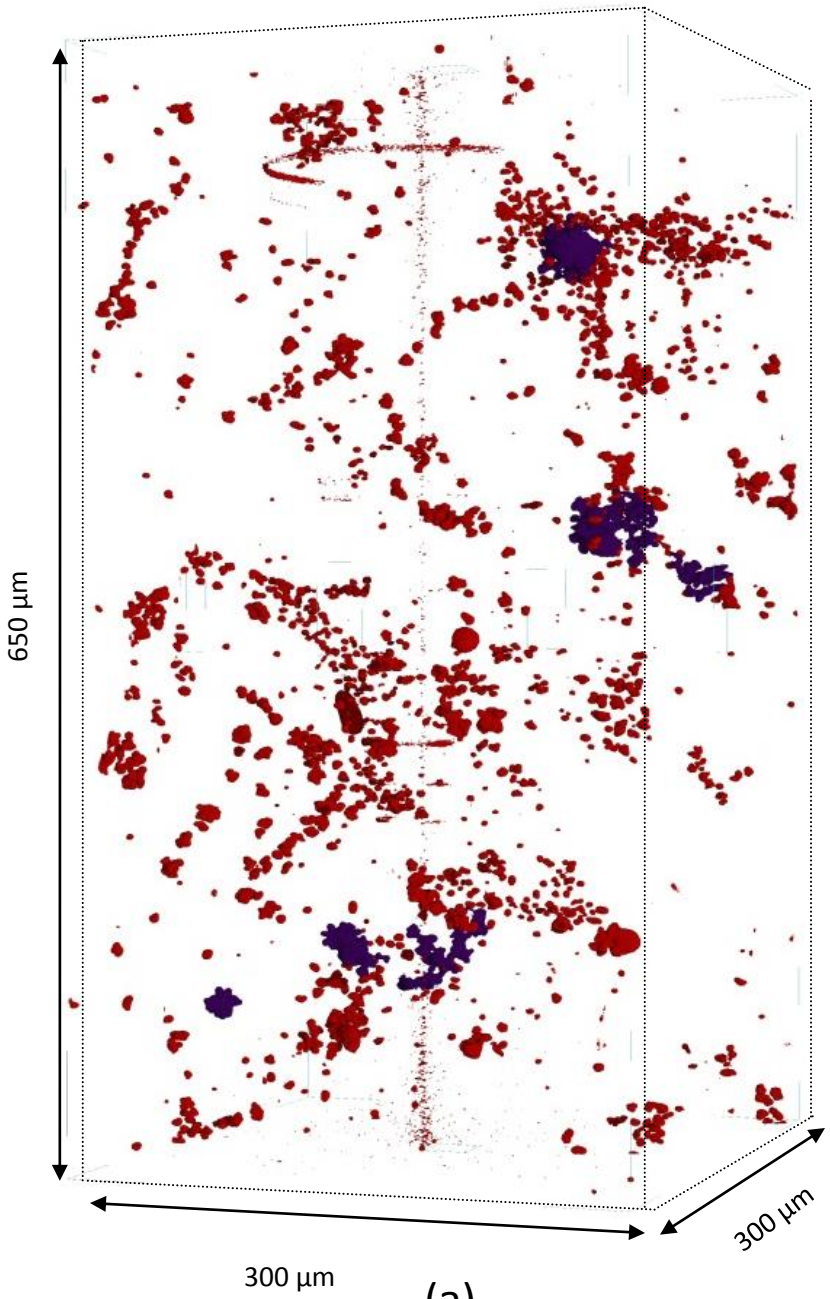

(a)

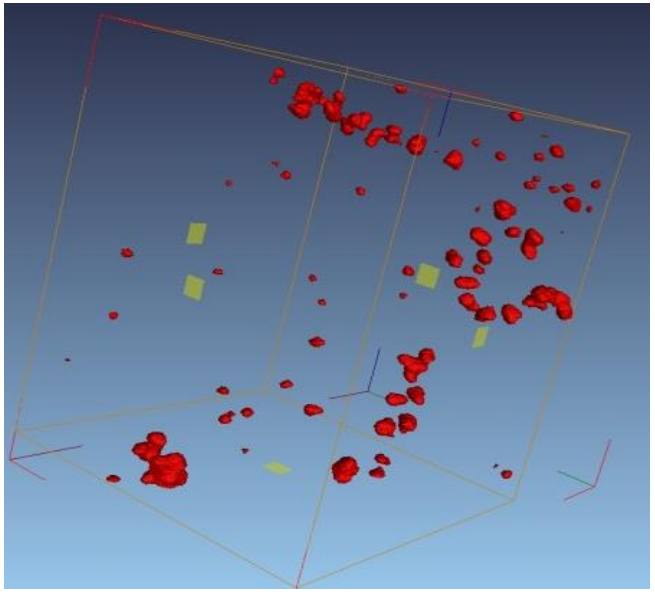

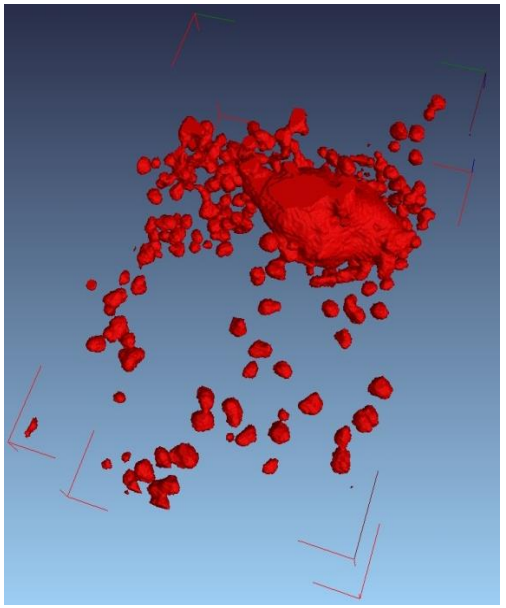

(b)

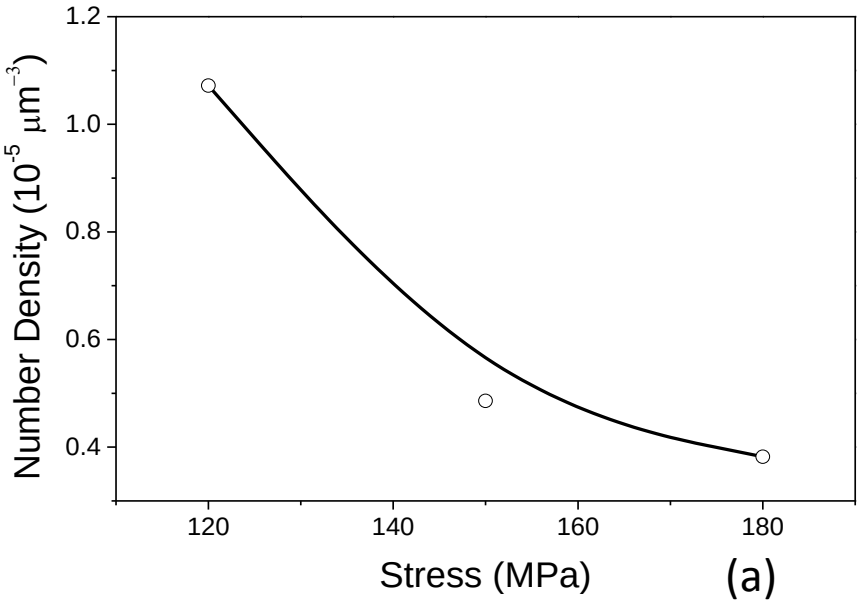
Number Density (10^{-5} μm^{-3})
1.2
1.0
0.8
0.6
0.4
120
140
160
180
Stress (MPa)
(a)

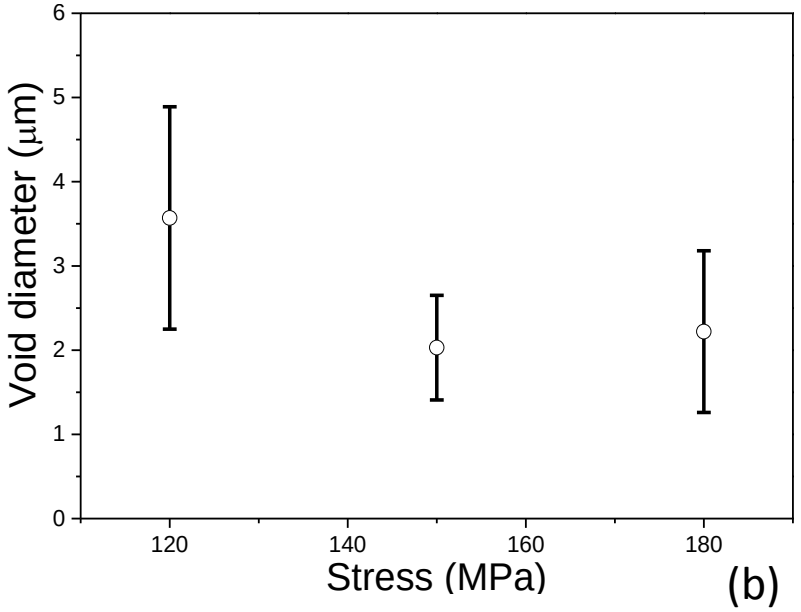
Void diameter (μm)
6
5
4
3
2
1
0
120
140
160
180
Stress (MPa)
(b)

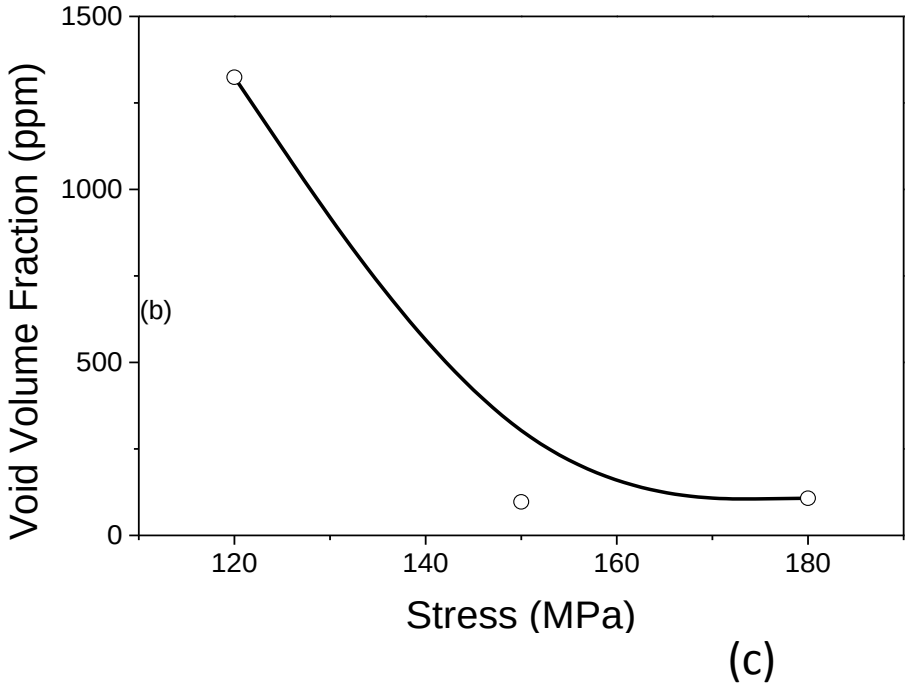
Void Volume Fraction (ppm)
1500
1000
500
0
(b)
120
140
160
180
Stress (MPa)
(c)

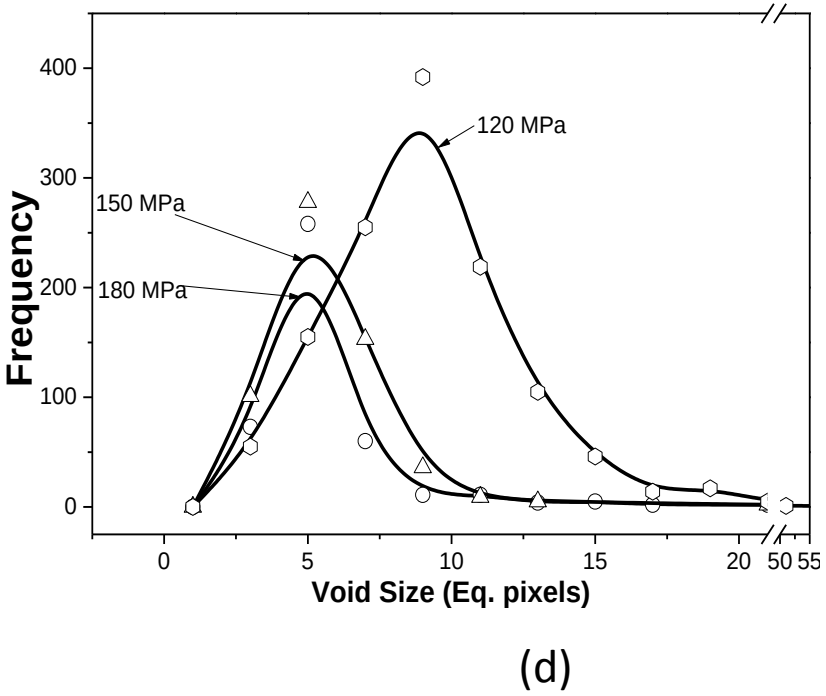
Frequency
400
300
200
100
0
120 MPa
150 MPa
180 MPa
0
5
10
15
20
50
55
Void Size (Eq. pixels)
(d)

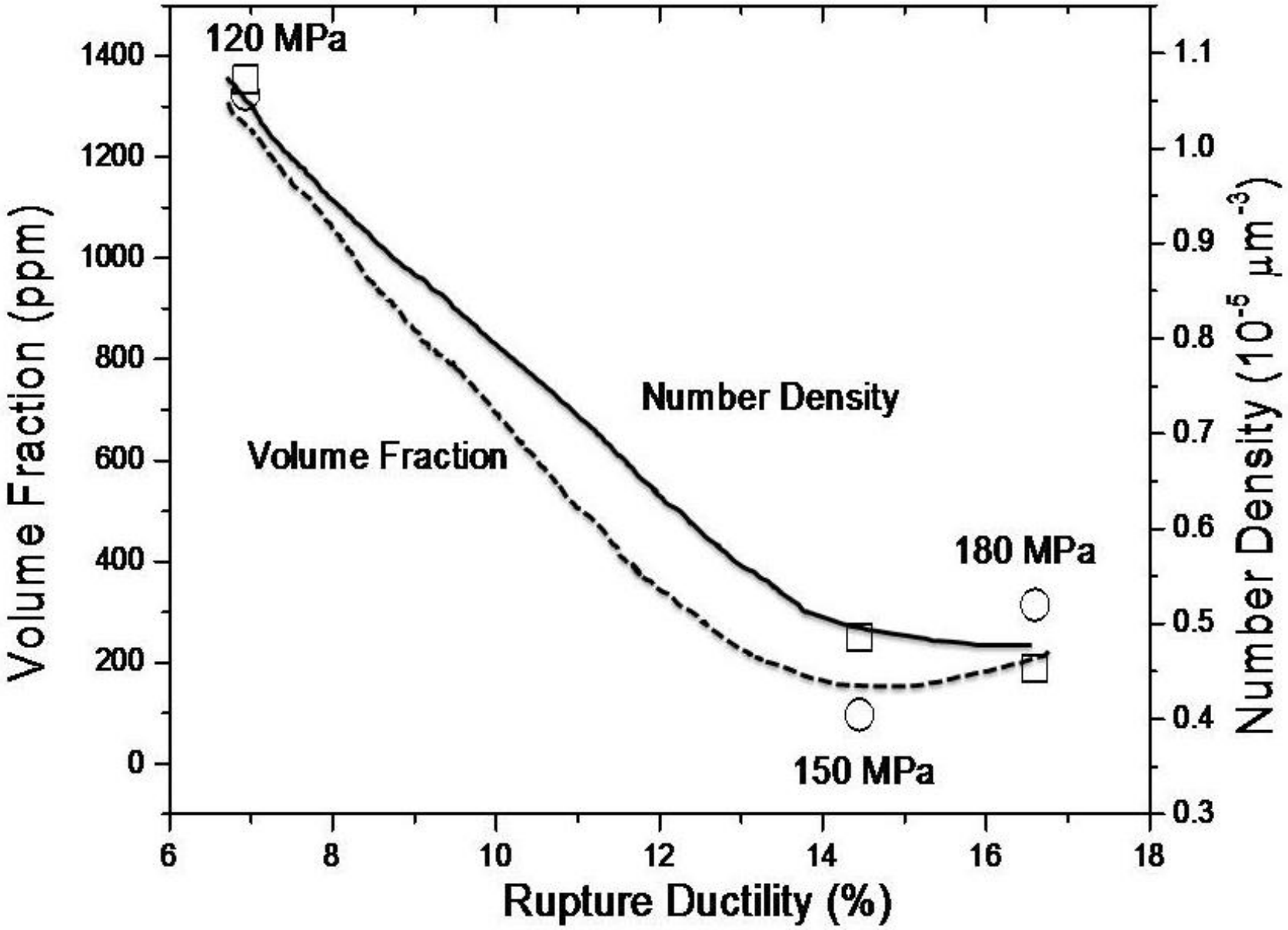
120 MPa
Number Density
Volume Fraction
180 MPa
150 MPa
Volume Fraction (ppm)
Number Density (10^{-5} μm^{-3})
Rupture Ductility (%)
0
200
400
600
800
1000
1200
1400
0.3
0.4
0.5
0.6
0.7
0.8
0.9
1.0
1.1
6
8
10
12
14
16
18

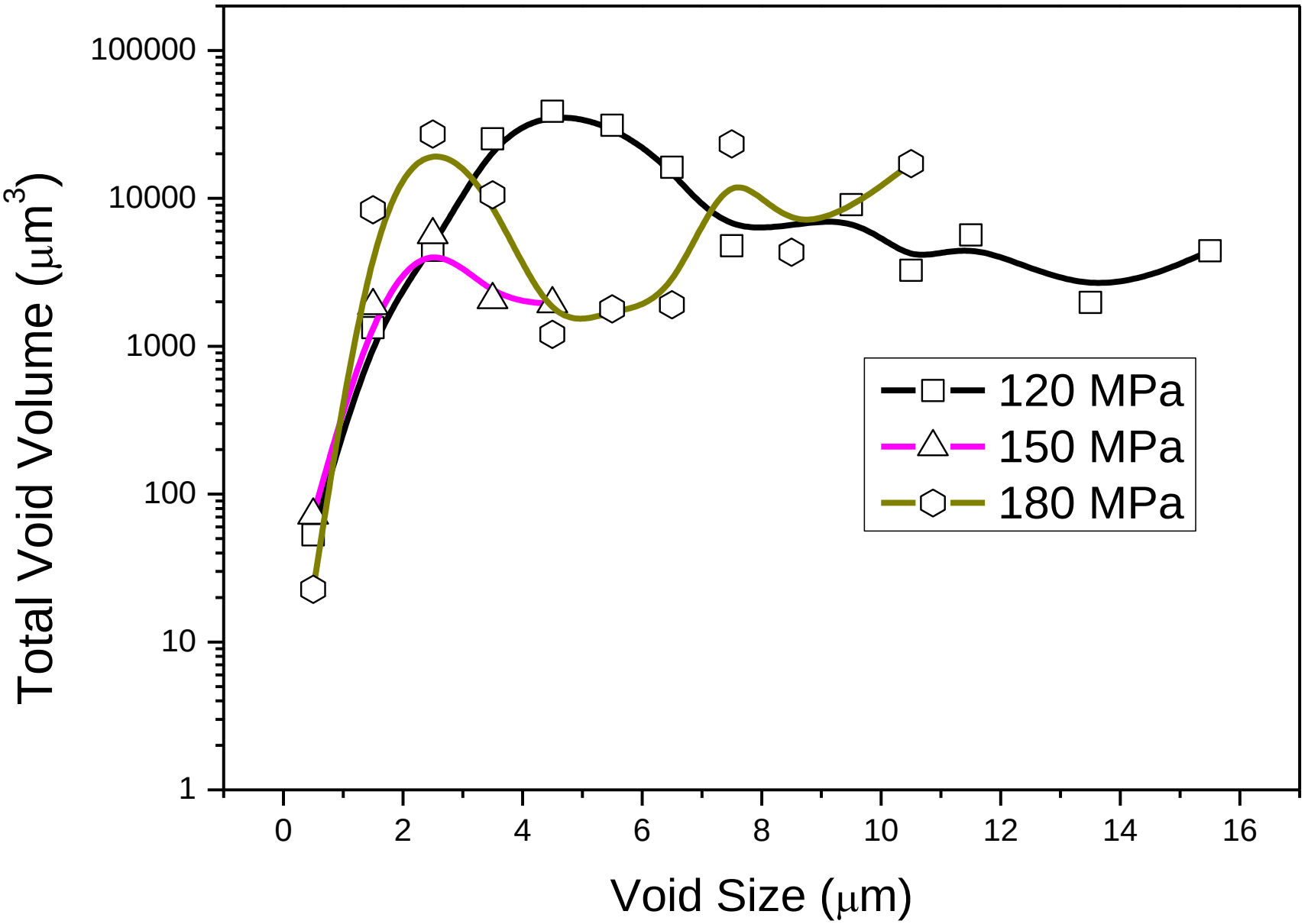
Total Void Volume (μm3)
100000
10000
1000
100
10
1
0
2
4
6
8
10
12
14
16
Void Size (μm)
120 MPa
150 MPa
180 MPa

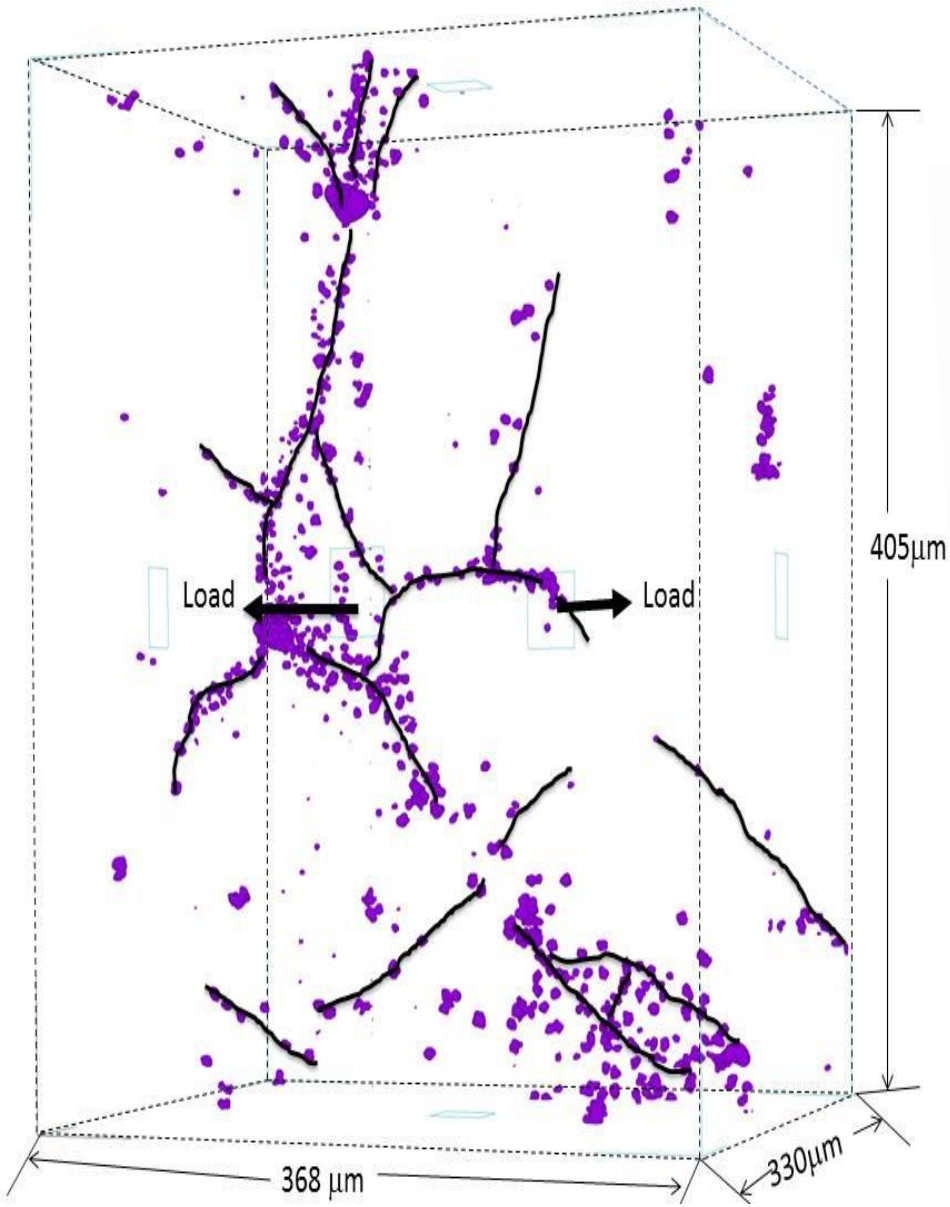

(a)

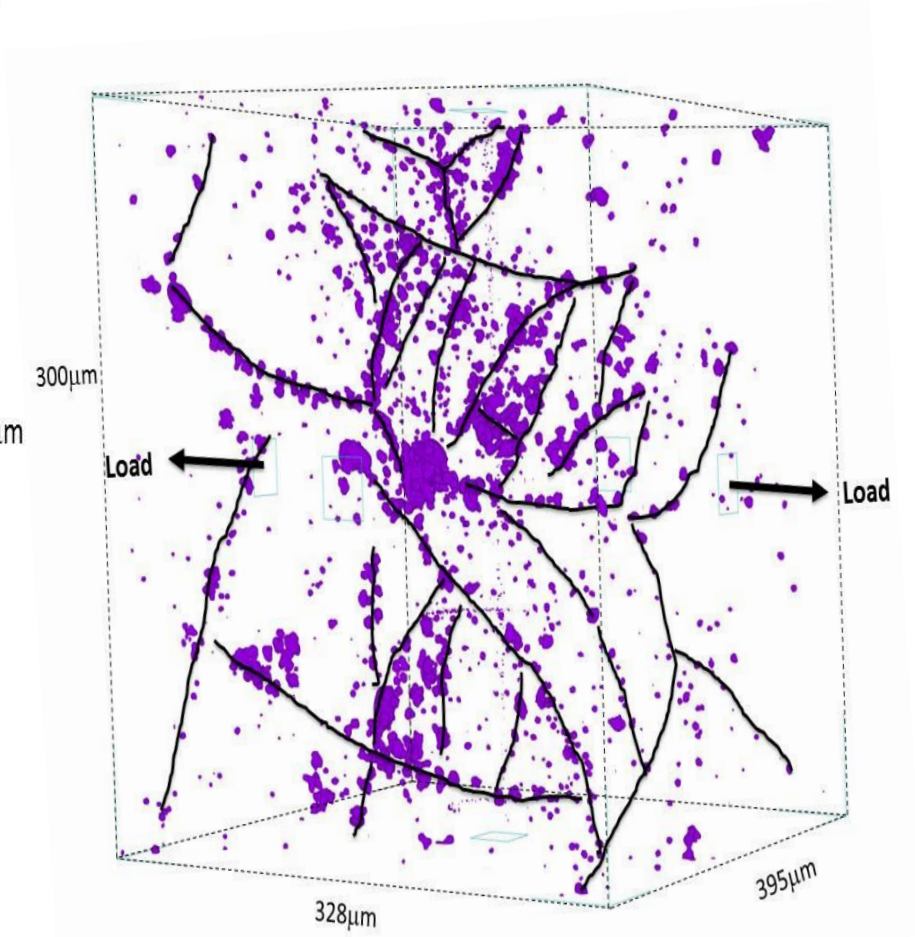

(b)